Theor Chem Acc (2006) 115: 308–321
DOI 10.1007/s00214-005-0045-5

REGULAR ARTICLE

Nilesh R. Dhuaml · Shridhar P. Gejji

Theoretical investigations on structure, electrostatics potentials and vibrational frequencies of Li^+–CH_3–O–$(CH_2$–CH_2–O$)_n$–CH_3(n = 3–7) conformers

Received: 11 August 2005 / Accepted: 31 August 2005 / Published online: 12 January 2006

Abstract Electronic structure, charge distributions and vibrational characteristics of $CH_3O(CH_2CH_2O)_nCH_3$ (n = 3–7) have been derived using the ab initio Hartree Fock and density functional calculations. For tri- to hexaglymes the lowest energy conformers have *trans*- conformation around the C–C and C–O bonds of the backbone. For heptaglyme (n = 7 in the series), however, *gauche*-conformation around the C–C bonds renders more stability to the conformer and turns out to be 10.1 kJ mol^{-1} lower in energy relative to the conformer having *trans*-orientation around the C–C and C–O bonds. The molecular electrostatic potential topographical investigations reveal deeper minima for the ether oxygen in conformers having the gauche conformation around the C–C bonds over those for the *trans*-conformers. A change from *trans*- to *gauche*-conformation around the C–C bonds of the lowest energy conformer of heptaglyme engenders a triplet of intense bands ∼1,150 cm^{-1} in the vibrational spectra. Theoretical calculations predict that Li^+ binds strongly to the heptaglyme conformer in the above series. The frequency shifts in the vibrational spectra of $CH_3O(CH_2CH_2O)_nCH_3$ − Li^+ (n = 3–7) conformers have been discussed.

1 Introduction

Poly(ethylene oxide) (PEO) oligomers represented by the formula $H_3CO(CH_2CH_2O)_nCH_3$ dissolve a variety of ionic salts, such as $LiCF_3SO_3$ [1] or $Li(CF_3SO_2)_2N$ [2,3] to form solid polymer electrolytes (SPE) [4], exhibit high ionic conductivity [5,6], which facilitate their use in fuel cells, secondary batteries and other electrochemical devices [7]. The ion–polymer and ion–ion interactions or ionic association in these systems are important in the ion transport phenomenon [8–10]. Among these ionic associations, formation of ion-pairs or ion triplets can be studied experimentally using the infrared and Raman spectroscopy [11–13]. Interestingly the cation–polymer interactions result in the polymer segmental motion of the polymers [14]. In order to understand the relationship between the ionic transport and local structure of the polymer matrix at the molecular level, ab inito quantum chemical calculations have been explored in the recent literature [15–18]. The coordination of metal ion to ether oxygens of poly-ethers and the accompanying change in the chain conformation has consequently been of a great importance in understanding the transport properties of the electrolytes [19]. With this view a number of theoretical studies have been aimed to characterize the ion–polymer and ion–ion interactions in PEO oligomers bound by novel weakly coordinating salts. As a pursuit of this ab initio calculations on the lithium–diglyme complexes representing different coordination by two or three ether oxygens with lithium ion have been carried out [14,20]. These calculations have shown that complexes with either two or three ether oxygens interacting with the metal ion yield as stationary point geometries on the potential energy surface (PES), which have been identified as local minima. On the other hand the structure wherein Li^+ coordinates to a single oxygen of *trans*-conformer of diglyme turns out to be a transition state (saddle point of order 1) on the PES. It should be remarked here that the *gauche*-conformation around the C–C bond of diglyme is favoured in the 1:1 lithium-diglyme ion-pair. Johansson et al. [19] have carried out HF/3–21G calculations on the Li^+-triglyme complex and suggested a tetradentate structure for lithium-triglyme. Johansson et al. [20] have further investigated 1:1 ion pair geometries of lithium and tetra-, penta-, or hexaglymes using the ab initio molecular orbital calculations at the Hartree–Fock theory employing the 3–21G* basis set. These calculations have shown that the lithium cation binds strongly to hexaglyme than the lower PEO oligomers. In the recent literature, the elementary steps in lithium ion transport along a PEO chain has been modelled using the quantum chemical calculations [21]. Raman scattering and infrared transmission spectroscopy experiments

N.R. Dhuaml · S.P. Gejji (✉)
Department of Chemistry,
University of Pune,
Pune 411 007, India
E-mail: spgejji@chem.unipune.ernet.in
Fax: +91-20-25691728

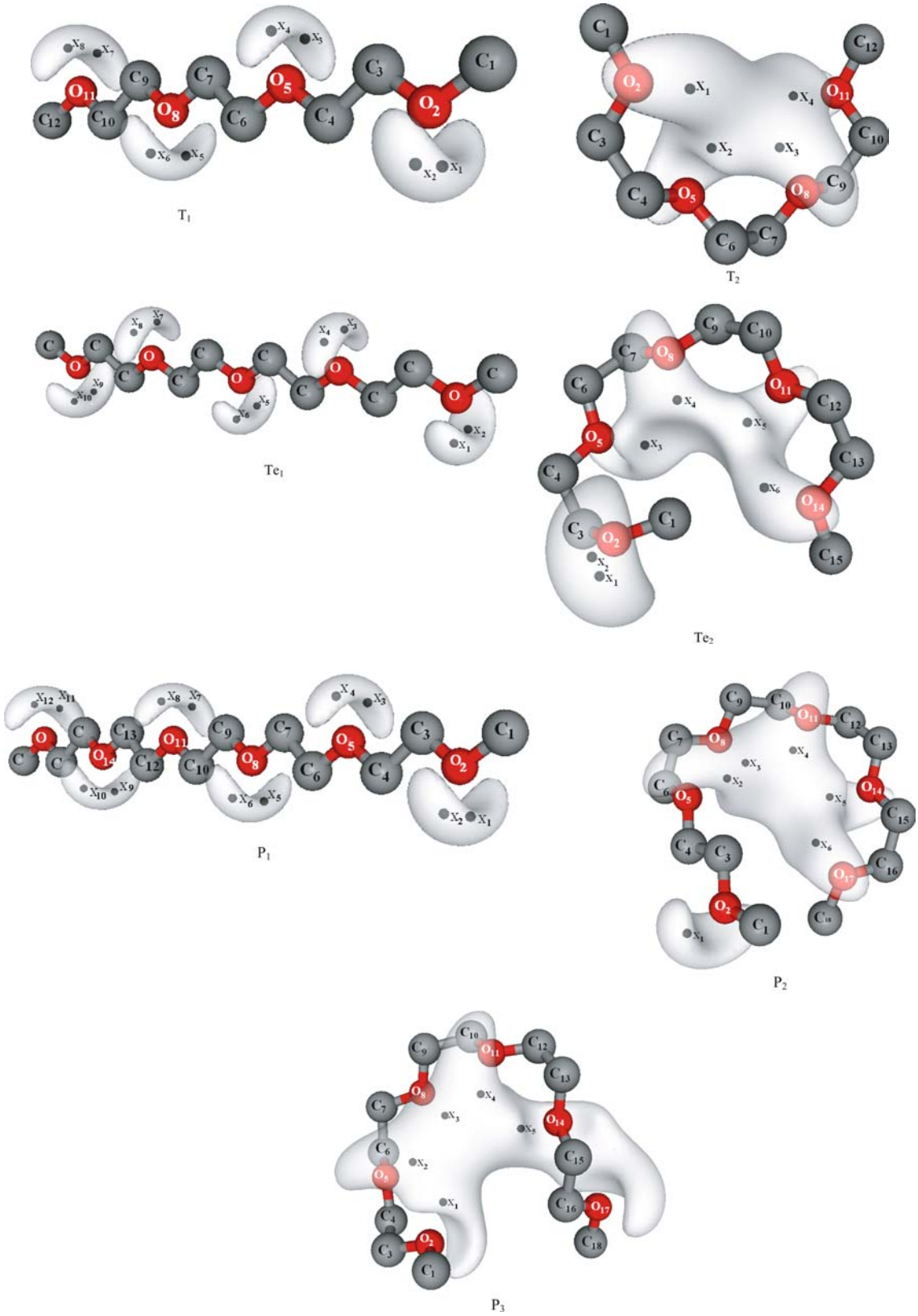

Fig. 1 MESP ($V = -131.3\,\mathrm{kJ\,mol^{-1}}$) isosurfaces for the different conformers of $CH_3O(CH_2CH_2O)_nCH_3$ (n = 3–7) (Hydrogens omitted for clarity)

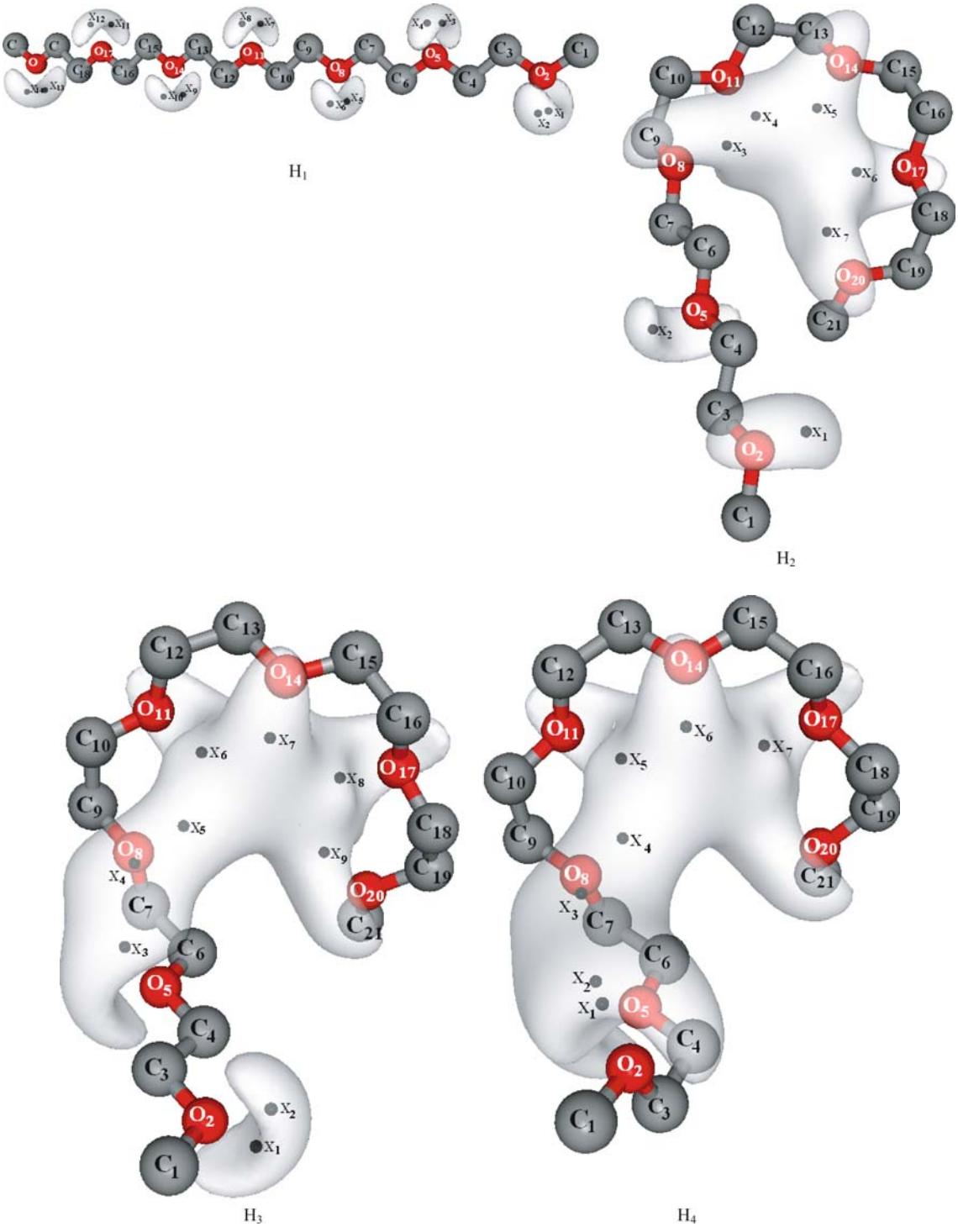

Fig. 1 (contd.)

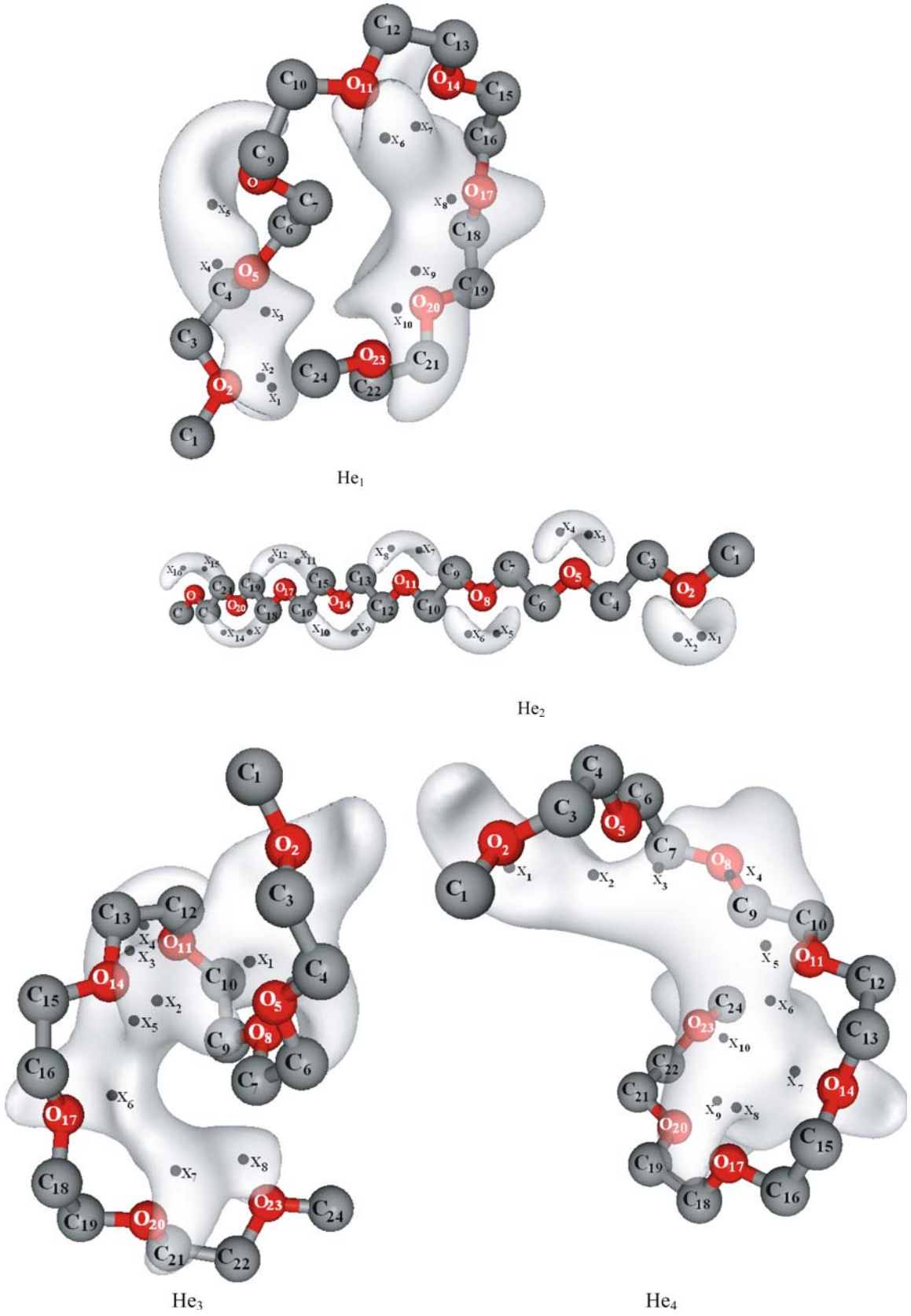

Fig. 1 (contd.)

Table 1 Relative stabilization (ΔE) in kJ mol^{-1} for the conformers of $CH_3O(CH_2CH_2O)_nCH_3$(n = 3–7)

	Δ E
T_1	0.0 (0. 0)
T_2	8.7 (8.0)
Te_1	0.0 (0.0)
Te_2	0.4 (1.8)
P_1	0.0 (0.0)
P_2	2.5 (4.7)
P_3	10.7 (11.4)
H_1	0.0 (0.0)
H_2	3.0 (5.1)
H_3	9.8 (10.4)
H_4	14.3 (14.7)
Hp_1	0.0 (0.0)
Hp_2	10.1 (6.5)
Hp_3	13.9 (14.4)
Hp_4	21.0 (18.9)

ZPE corrected values are given in parentheses

have suggested that the complexation of PEO oligomers with lithium trifluoromethanesulphonate ($LiCF_3SO_3$) engenders a change in conformation about the C–C and C–O bonds of the oligomer [22–27]. In the vibrational spectra of the diglyme-$LiCF_3SO_3$ intense bands of CH_2 bending appear at higher frequencies with the increasing salt concentration. Thus, it may be inferred that both the conformational change and the ionic association influence the vibrational spectra of diglyme. Since the affinity of cation (Li^+) towards the $CF_3SO_3^-$, $(CF_3SO_2)_2N^-$ and $(CF_3SO_2)_2CH^-$ anions arises mainly due to the electrostatic effect while the contribution from the charge transfer interactions are of less significance [28]. It is important to probe the role of molecular electrostatics potential to understand the cation coordination in the complex formation. The scalar fields like the molecular electrostatic potential (MESP), which is comprised of bare nuclear potential and the electronic contributions, brings about the effective localization of the electron-rich regions of the molecular system. Gejji et al. have demonstrated how the MESP topography can be used as a harbinger to cation coordination using the triflate anion as a model system. The strength of such cation–anion interactions forming an neutral ion pair can also be adjudged from the charge enclosed within a given MESP isosurface. Thus, the MESP topography has been explored to understand the molecular interactions in different ion -pairs in the solid polymer electrolytes [29–32].

As a pursuit of this in the present work we systematically investigate the binding patterns and the vibrational spectra of the tri- to heptaglyme and their lithium complexes using the MESP topography as a tool. The computational method has been outlined below.

2 Computational method

LCAO-MO-SCF restricted Hartree–Fock (HF) calculations were carried out on the different conformers of $H_3C–O–(CH_2–CH_2–O)_n–CH_3$ (n = 3–7) using the GAUSSIAN 03 program [33]. The internally stored 6–31G(d, p) basis set was used. Different conformers of the oligomer were generated by either a single C–C or C–O bond rotation or by simultaneous rotations around the central C–C as well as C–O bonds of the all *trans* conformer of $H_3C–O–(CH_2–CH_2–O)_n–CH_3$. The MESP, $V(\mathbf{r})$, at a point $\mathbf{r}$ due to a molecular

Table 2 Bond lengths (Å) for the different conformers of $CH_3O(CH_2CH_2O)_nCH_3$(n = 3–7)

	T_1	T_2	Te_1	Te_2	P_1	P_2	P_3	H_1	H_2	H_3	H_4	Hp_1	Hp_2	Hp_3	Hp_4
$r(C_1–O_2)$	1.412	1.391	1.412	1.426	1.412	1.415	1.412	1.412	1.411	1.410	1.409	1.411	1.412	1.415	1.411
$r(O_2–C_3)$	1.414	1.392	1.414	1.411	1.413	1.420	1.414	1.413	1.414	1.416	1.413	1.416	1.413	1.421	1.416
$r(C_3–C_4)$	1.521	1.511	1.521	1.524	1.521	1.521	1.515	1.521	1.521	1.521	1.515	1.515	1.521	1.530	1.515
$r(C_4–O_5)$	1.415	1.393	1.415	1.417	1.415	1.414	1.412	1.415	1.418	1.415	1.414	1.410	1.415	1.423	1.411
$r(O_5–C_6)$	1.415	1.392	1.415	1.411	1.415	1.412	1.410	1.414	1.422	1.415	1.415	1.423	1.415	1.415	1.416
$r(C_6–C_7)$	1.521	1.511	1.521	1.516	1.521	1.517	1.516	1.521	1.512	1.515	1.515	1.511	1.521	1.524	1.514
$r(C_7–O_8)$	1.415	1.392	1.415	1.414	1.415	1.413	1.413	1.415	1.413	1.412	1.411	1.433	1.415	1.419	1.416
$r(O_8–C_9)$	1.415	1.393	1.415	1.413	1.415	1.411	1.411	1.415	1.412	1.410	1.410	1.412	1.415	1.420	1.415
$r(C_9–C_{10})$	1.521	1.511	1.521	1.516	1.521	1.516	1.516	1.521	1.517	1.516	1.516	1.524	1.521	1.522	1.515
$r(C_{10}–O_{11})$	1.414	1.392	1.415	1.414	1.415	1.412	1.413	1.415	1.413	1.413	1.413	1.417	1.415	1.417	1.411
$r(O_{11}–C_{12})$	1.412	1.391	1.415	1.414	1.415	1.412	1.412	1.415	1.411	1.410	1.411	1.410	1.415	1.422	1.409
$r(C_{12}–C_{13})$			1.521	1.515	1.521	1.516	1.516	1.521	1.516	1.516	1.516	1.516	1.521	1.515	1.516
$r(C_{13}–O_{14})$			1.414	1.413	1.415	1.413	1.415	1.415	1.412	1.413	1.412	1.414	1.415	1.415	1.412
$r(O_{14}–C_{15})$			1.412	1.412	1.415	1.413	1.413	1.415	1.412	1.412	1.411	1.413	1.415	1.419	1.412
$r(C_{15}–C_{16})$					1.521	1.514	1.515	1.521	1.516	1.517	1.517	1.516	1.521	1.514	1.517
$r(C_{16}–O_{17})$					1.413	1.414	1.415	1.415	1.413	1.415	1.415	1.414	1.415	1.415	1.412
$r(O_{17}–C_{18})$					1.412	1.416	1.412	1.415	1.413	1.413	1.413	1.414	1.415	1.413	1.413
$r(C_{18}–C_{19})$								1.521	1.516	1.515	1.515	1.516	1.521	1.516	1.518
$r(C_{19}–O_{20})$								1.413	1.414	1.415	1.415	1.412	1.415	1.412	1.413
$r(O_{20}–C_{21})$								1.412	1.415	1.412	1.412	1.419	1.415	1.416	1.418
$r(C_{21}–C_{22})$												1.514	1.521	1.524	1.515
$r(C_{22}–O_{23})$												1.490	1.413	1.411	1.417
$r(O_{23}–C_{24})$												1.416	1.412	1.426	1.411

Table 3 MESP values (kJ mol^{-1}) at the critical points (minima) in the different conformers of $CH_3O(CH_2CH_2O)_nCH_3$ (n = 3–7)

	X_1	X_2	X_3	X_4	X_5	X_6	X_7	X_8	X_9	X_{10}	X_{11}	X_{12}	X_{13}	X_{14}	X_{15}	X_{16}
T_1	−214.8	−214.8	−197.1	−197.1	−197.1	−197.1	−214.7	−214.8								
T_2	−257.3	−254.4	−255.4	−249.9	−220.6	−221.1										
Te_1	−214.6	−214.6	−196.1	−169.1	−195.7	−195.7	−196.2	−196.1	−214.6	−214.5						
Te_2	−253.2	−252.1	−226.0	−248.0	−247.4	−226.0	−219.7	−219.1	−218.8							
P_1	−214.1	−214.1	−195.7	−195.7	−194.5	−194.4	−194.5	−194.5	−195.7	−195.7	−214.2	−214.2				
P_2	−250.8	−252.2	−246.9	−212.9	−245.7	−218.8	−219.3									
P_3	−305.5	−302.7	−240.3	−272.7	−280.3	−293.3										
H_1	−214.1	−214.1	−195.4	−195.3	−194.1	−194.1	−193.3	−193.3	−194.2	−194.2	−192.8	−192.8	−214.0	−214.0		
H_2	−210.8	−243.5	−248.4	−244.4	−250.1	−212.4	−226.3	−224.9								
H_3	−303.0	−294.6	−304.3	−228.2	−221.5	−273.7	−280.2									
H_4	−294.7	−277.7	−266.7	−233.6	−234.2	−292.9	−307.4	−304.9	−273.0							
Hp_1	−210.3	−243.0	−249.3	−247.8	−243.4	−202.9	−204.3	−224.7	−244.6							
Hp_2	−214.0	−214.0	−195.4	−195.4	−193.8	−193.9	−193.1	−193.1	−193.0	−193.0	−193.9	−193.9	−195.4	−195.4	−214.0	−214.0
Hp_3	−297.6	−282.0	−261.6	−240.9	−228.5	−258.1	−271.2	−287.7	−284.6	−292.5						
Hp_4	−298.5	−273.4	−287.1	−279.0	−276.4	−244.2	−287.0	−281.9	−268.0	−259.4						

Table 4 Selected B3LYP vibrational frequencies for the lowest energy conformer of $CH_3O(CH_2CH_2O)_nCH_3$ (n = 3–7)

Assignment	T_1	Te_1	P_1	H_1	Hp_1
CH_2 scissor	1,534 (22)	1,536 (31)	1,537 (40)	1,537 (50)	1,505 (23)
CH_2 rock	1,341 (91)	1,337 (121)	1,335 (151)	1,334 (182)	1,392 (74)
					1,387 (169)
CH_2 twist	1,249 (26)	1,250 (32)	1,251 (39)	1,251 (45)	1,280 (30)
	1,235 (115)	1,235 (110)	1,235 (110)	1,235 (108)	1,191 (36)
C–O stretch	1,185 (669)	1,186 (694)	1,186 (450)	1,187 (187)	1,174 (202)
	1,174 (185)	1,179 (440)	1,182 (940)	1,183 (1429)	1,171 (134)
			1,172 (81)	1,176 (198)	1,159 (177)
CH_2 wag					1,154 (175)
					1,148 (137)
					1,145 (219)
CC + CO stretch	981 (112)	982 (134)	984 (154)	984 (176)	977 (84)
					974 (46)

system with nuclear charges $\{Z_A\}$ located at $\{\mathbf{R}_A\}$ and electron density $\rho(\mathbf{r})$ is defined by

$$V(\mathbf{r}) = \sum_{A=1}^{N} \frac{Z_A}{|\mathbf{r} - \mathbf{R}_A|} - \int \frac{\rho(\mathbf{r}')d^3\mathbf{r}'}{|\mathbf{r} - \mathbf{r}'|}, \quad (1)$$

where N denotes the total number of nuclei in the molecule. The first term in Eq. (1) refers to the bare nuclear potential and the second term to the electronic contribution. The topography of MESP is mapped by examining the eigenvalues of the Hessian matrix at the point where the gradient $V(\mathbf{r})$ vanishes. The MESP critical points (CPs) can be characterized from its rank and signature (excess of positive eigenvalues over negative ones). Thus the minima are denoted as (3, +3), maxima are denoted as (3, −3) and two types of saddles are represented by (3, −1) and (3, +1). The MESP CPs were visualized by using the package UNIVIS 2000 [34]. The MESP minima near ether oxygens are employed as the potential cation binding sites for the oligomer. To begin with, the lithium ion was placed in the vicinity of the deepest MESP minima and the structure of the oligomer-metal ion was optimized using the HF/6-31G(d, p) theory. These optimized geometries were subsequently subjected to optimization in the hybrid density functional theory employing Becke's three parameter exchange with Lee, Yang, Parr's correlation functional (B3LYP) method [35,36]. The stationary point geometries thus derived were confirmed to be the local minima on the PES from the negative eigenvalues of the Hessian matrix. Cation binding energies of different $CH_3(OCH_2CH_2)_nOCH3$ (n = 3–7) conformers have been calculated by subtracting the sum of the electronic energies of the individual glyme and the Li^+ ion from the total SCF electronic energies of the ion pair complexes. Normal vibrations from the B3LYP theory were assigned by visualizing the displacement of atoms around their equilibrium positions using the programme UNIVIS–2000 [34].

3 Results and discussion

Different conformers were generated by rotations around the C–C and C–O bonds of the *trans*- conformer of CH_3–O–$(CH_2$–CH_2–O$)_n$–CH_3 (n = 3–7) the series. B3LYP-optimized geometries of some of the conformers of tri- to hepta glymes are displayed in Fig. 1. Conformers having either *trans*- or *gauche*-conformation around either C–C or C–O bonds were considered since these are more relevant for

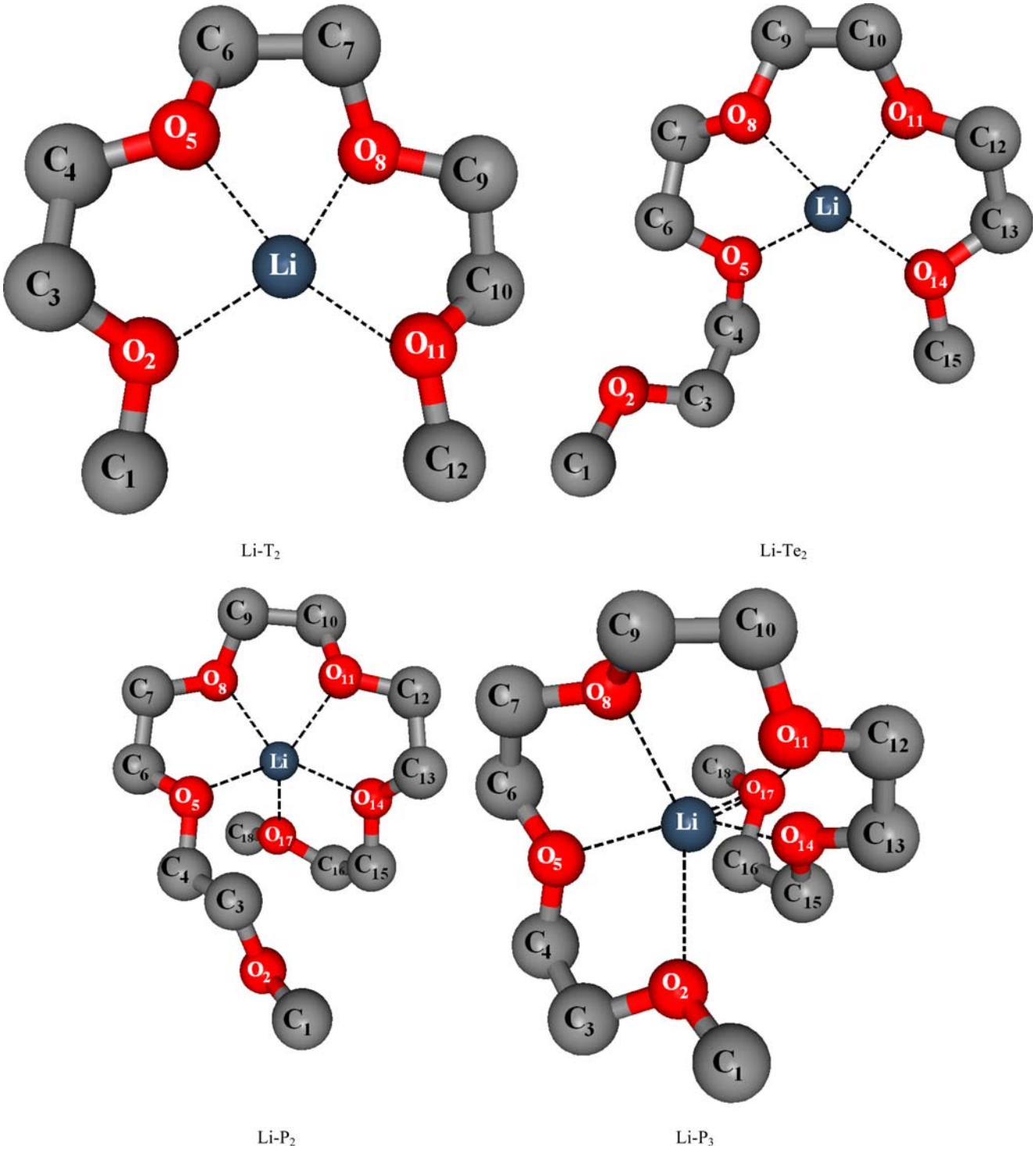

Fig. 2 Optimized geometries of the conformers of $CH_3O(CH_2CH_2O)_nCH_3$–Li^+ (n = 3–7) (Hydrogens omitted for clarity)

the cation binding. Thus, the relative stabilization energies of different tri- to heptaglymes conformers are given in Table 1 along with the zero point energy corrected values in parentheses. Among the different conformers of tri- to hexaglymes the lowest energy conformer prefers to have *trans*-conformation around the C–C bonds and the C–O bonds as well. For heptaglyme (n = 7), however, the lowest energy conformer prefers to have the *gauch*-conformation around the C–C bonds of the backbone of the oligomer. The *trans*- conformer in this case is destabilized by 10.1 kJ mol^{-1} relative to the lowest energy conformer. Large repulsions of ether oxygens in the tri- to hexaglyme conformers as in, the structures possessing the *gauche*-conformation around the C–C bonds, are destabilized largely over all the corresponding *trans*- (*trans*-con-

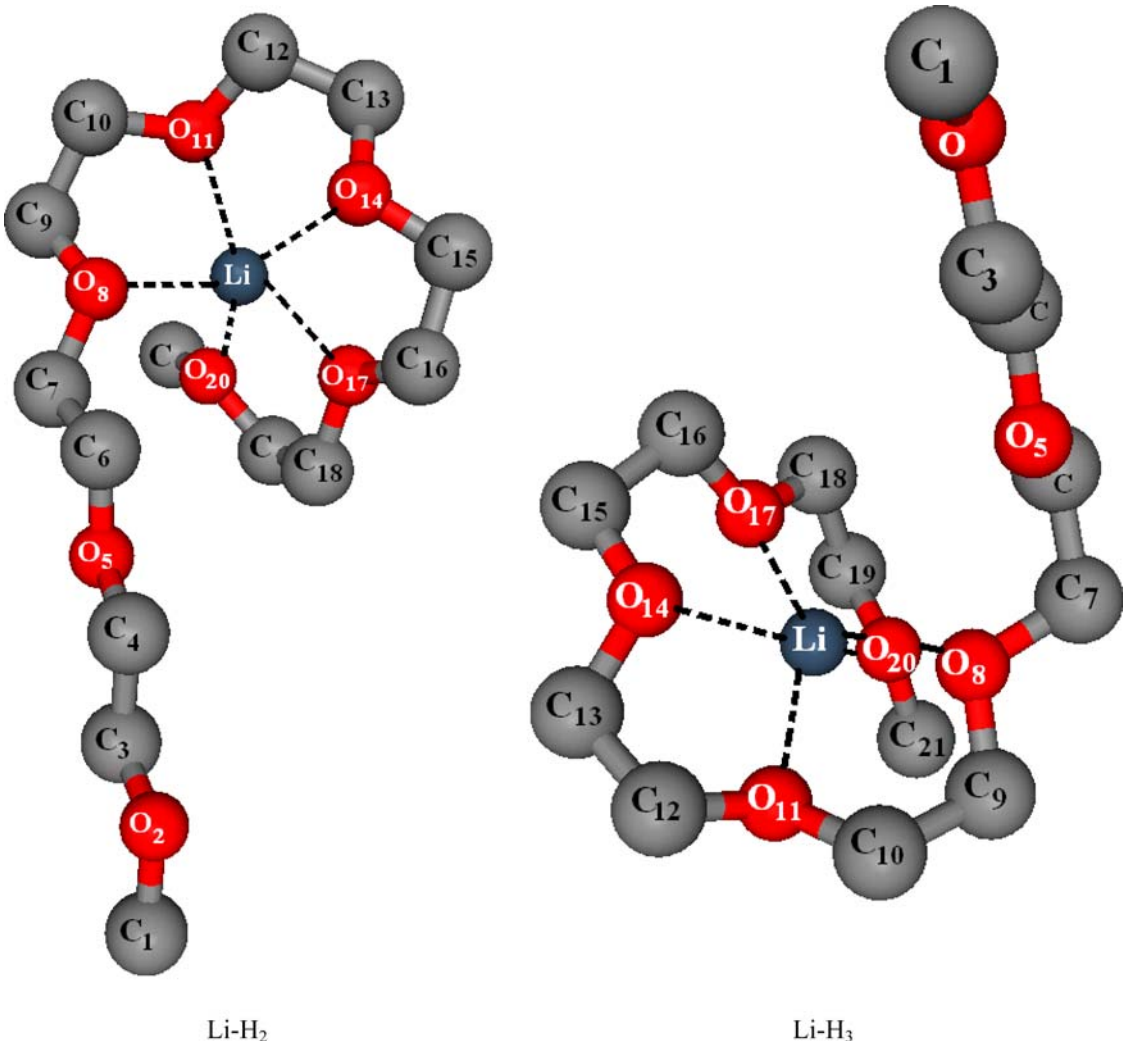

Fig. 2 (contd.)

formation around the C–C and C–O bonds of the backbone of the oligomer) conformers in the gas phase.

The geometrical parameters of different conformers in different PEO oligomers are displayed in Table 2. As revealed from the table, lowest energy conformers emerge with longer CO bond distances.

As noted earlier MESP brings about the effective localization of the electron-rich regions of the molecular system. The MESP topography in a series of PEO oligomers encompassing from tri- to heptaglyme conformers have been calculated from the Hartree–Fock wavefunction using Eq. (1) presented in Section II. MESP isosurfaces ($V = -131.3$ kJ mol^{-1}) of different $CH_3O(CH_2CH_2O)_nCH_3$ ($n = 3$–7) conformers are depicted in Fig. 1. As may be noticed readily among different conformers of the series of glymes, the volume enclosed by the MESP isosurface for T_2, Te_2, P_3, H_4 and Hp_4 conformers turn out to be relatively large compared to those in all the corresponding *trans*-conformers. Thus, the smaller localized electron-rich regions near the oxygen atoms revealing the shallow MESP minimum are observed for the lowest energy conformers (Fig. 1). On the other hand for tri- to heptaglymes, the *gauche*-conformation around the C–C backbone of the PEO oligomer engenders the deeper MESP minima near ether oxygens implying stronger cation binding. MESP minima in different PEO oligomers are summarized in Table 3.

The characteristics of vibrations of PEO oligomer in these SPE, in particular the frequency shifts of these vibrations provide insights for the ion–polymer interactions. In order to understand these interactions at the molecular level we have analyzed the frequencies of normal vibrations derived from the B3LYP theory. Selected vibrational frequencies of the lowest energy conformers in a series of tri- to heptaglymes in the 900 –1,540 cm^{-1} region, are displayed in Table 4. As may readily be noticed the 1,534 cm^{-1} CH_2 scissor appears in the *trans*-conformers of tri- to hexaglyme and is nearly insensitive to the increase of oligomer chain length. The conformational change from *trans* to *gauche* around the C–C bond in the heptaglyme ($n = 7$ in above series), however, shifts this vibration to 1,505 cm^{-1}. The intense CH_2

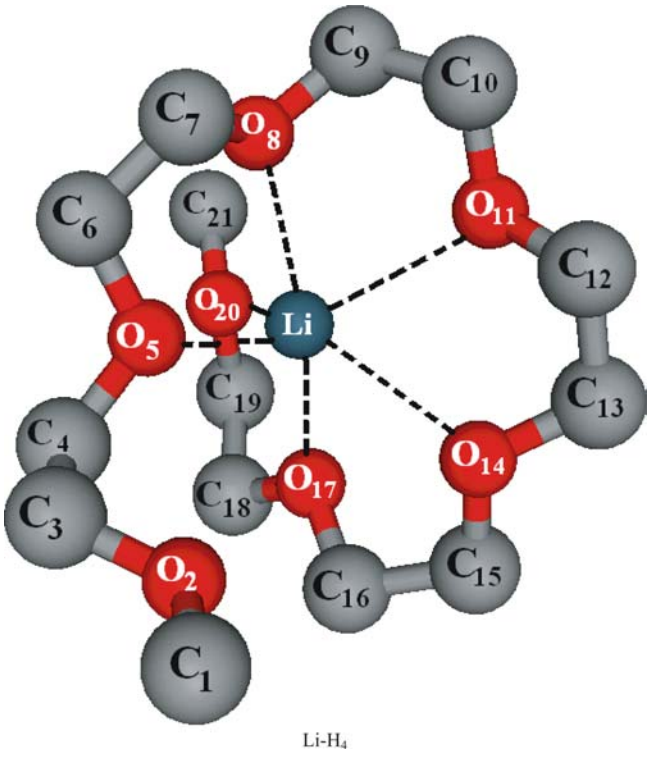

Fig. 2 (contd.)

rocking vibration in T_1 to H_1 (Fig. 1) along tri- to hexaglyme conformers downshifts from 1,341 to 1,334 cm^{-1}. For heptaglyme the conformational change around the C–C bonds manifests in the appearance of new vibrations at 1,392 and 1,387 cm^{-1}, which are assigned to CH_2 rock vibrations. A near doublet of 1,249 and 1,235 cm^{-1} (separated by 14 cm^{-1}) has been predicted in the T_1 to H_1 conformers. For Hp_1 the separation of the corresponding 1,280 and 1,191 cm^{-1} vibrations increases to 89 cm^{-1}. A near triplet for intense CH_2 wag vibrations ~1,150 cm^{-1} emerge as a signature of the conformation a change around the C–C bond in Hp_1. Further, 974 and 977 cm^{-1} vibrations, assigned to CO stretching are predicted only in the Hp_1, and not in $T_1 - H_1$ conformers.

In the crystalline phase of polymer electrolyte all the *trans*-conformation around the C–O and C–C bonds is of minor importance [26]. We hereafter consider conformers possessing the *gauche*-conformation around the C–C bonds of a series of glymes (except for the methoxy and methyl groups at the terminal) as a reference for discussion of metal ion-induced changes in structure and vibrational spectra on metal ion coordination. B3LYP optimized geometries of the Li^+–CH_3 $O(CH_2CH_2O)_n$–CH_3 (n = 3–7) complexes with metal ion exhibiting different coordination number with ether oxygens are shown in Fig. 2. As may be noticed lithium ion is in tetradentate environment in tri- (overall C_{2v} symmetry) and tetraglyme complexes. Selected B3LYP geometrical parameters of the tri- and tetraglymes complexed with the Li^+ ion are given in Table 5. Coordination with the lithium ion cause large elongation (0.042 Å) for the $C_6 - O_5$ bond in T_2 and Te_2 conformers. Relatively stronger Li^+ binding for tetraglyme than triglyme has been inferred (Li–O_5 1.979 Å in Te_1 vs. 1.992 Å in T_1).P_2 and P_3 conformers of n = 5, exhibit pentadentate coordination for Li^+ and are displayed in Fig. 2. Except for C_6–O_5 bond, the elongation of CO bond in P_2 structure is larger than that in P_3, which suggests stronger cation-ether oxygen binding in the latter. The Li–O_{14} bond distances are contracted in both P_2 and P_3 conformers. MESP minima near the O_{14} oxygen in P_3 is deeper compared with those for the rest of the oxygen atoms and possibly facilitates stronger bonding with cation. In Li^+-hexa glyme ion pair pentadentate coordination has been noticed for the H_2 and H_3 structures whereas H_4 engenders hexadentate coordinated metal ion. Large weakening of C–O bonds in H_4 conformer compared to that in H_2 and H_3 conformers suggests stronger interaction with the metal ion in the H_4 conformer. In case of hexaglyme–Li ion pairs the metal ion heptaglyme ion pair shows hexadentate (Hp_2 and Hp_3) coordination and heptadenate (Hp_4) coordination with the latter having stronger binding towards the cation.

Calculated binding energies of different conformers of tri- to heptaglymes are reported in Table 6. It should be remarked here that tri- to heptaglyme high-energy conformers bind strongly to the metal ion and the binding energies accordingly increase from 461 to 529 kJ mol^{-1}. These cation binding energies depend on the O–Li distance and the number of coordinating oxygens as well. The largest binding energy of 529 kJ mol^{-1} has been predicted for the heptaglyme (Hp_4) and the trend: heptaglyme > hexaglyme > pentaglyme > tetraglyme, consistent with the inferences drawn from the MESP minima borns out in these ion pairs.

Consequences of metal ion coordination to the characteristic vibrations of glymes with varying chain length are discussed here. Selected B3LYP vibrational frequencies of the lowest energy Li^+ $CH_3O(CH_2CH_2O)_nCH_3$ (n = 3–7) ion pairs in 1,520 to 450 cm^{-1} region and the T_2, Te_2, P_3, H_4 and Hp_4 conformers are reported in Table 7,8. Thus intense 1,512 cm^{-1} (assigned to CH_2 scissor) vibration in these ion pairs turns out to be nearly insensitive to the number of OCH_2CH_2 units of the oligomer. The intense 1,397 cm^{-1} CH_2 rocking vibration in lithium–triglyme ion pair, however, downshifts to 1,388 cm^{-1} with increasing chain length of the oligomer. Further, two intense vibrations near 1,275 and 1,225 cm^{-1} are predicted in these glyme–cation ion pairs. These are assigned to CH_2 twist and get separated more with increasing number of ether oxygens interacting with a metal ion in the ion pair conformer. The C–O stretchings thus can be classified as: (a) for ether oxygens interacting with a metal ion and (b) those which are not. Accordingly a frequency downshift of the C–O stretching vibration in former can be correlated with the strength of O–Li interactions. These C–O vibrations are predicted in the range 1,148 to 1,028 cm^{-1}. As may be inferred the 1,028 cm^{-1} vibration in hexaglyme suggests stronger interaction of ether oxygens to Li^+. On the other hand for oxygens not participating in such interactions these stretching vibrations are in the

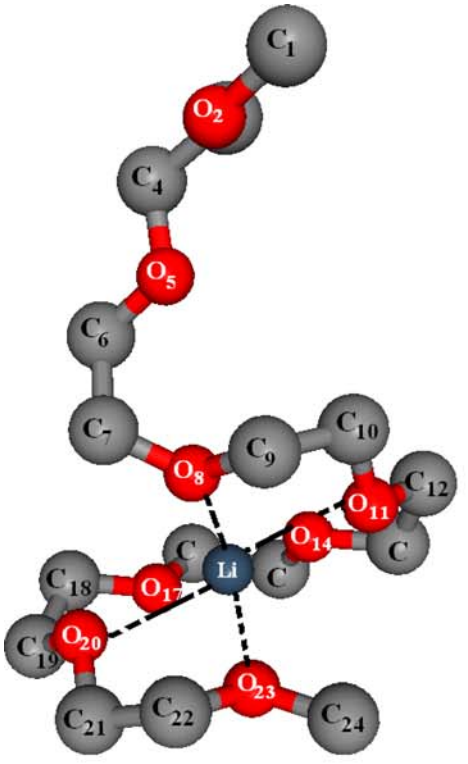

Li-Hp$_1$

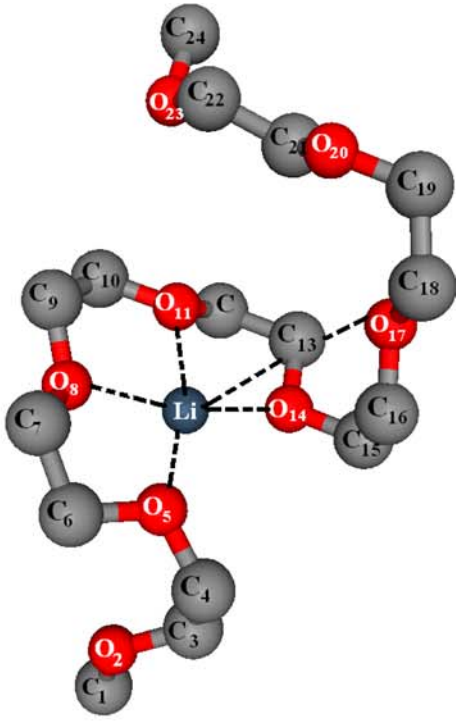

Li-Hp$_3$

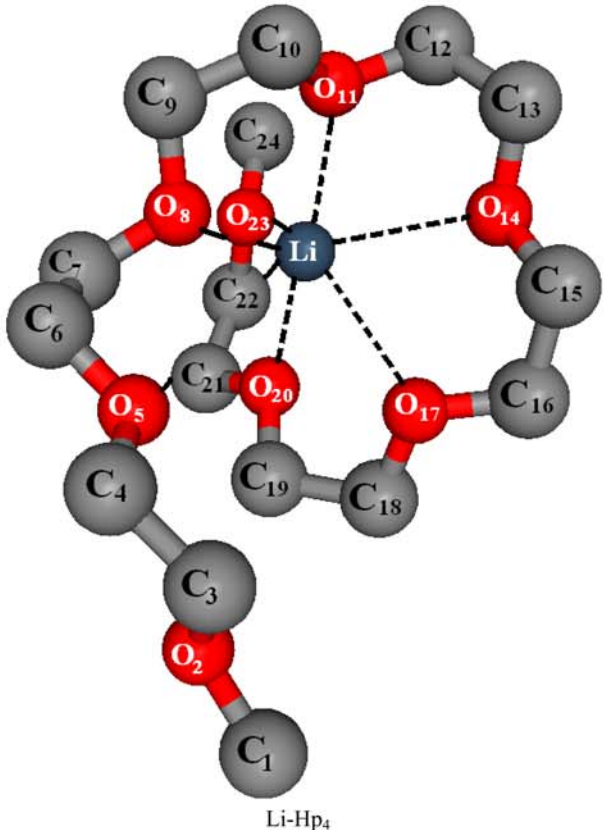

Li-Hp$_4$

Fig. 2 (contd.)

Table 5 Bond lengths (Å) for the different conformers of $CH_3O(CH_2CH_2O)_nCH_3$–Li^+ (n = 3–7)

	Li–T_2	Li–Te_2	Li–P_2	Li–P_3	Li–H_2	Li–H_3	Li–H_4	Li–Hp_1	Li–Hp_3	Li–Hp_4
C_1–O_2	1.434	1.422	1.422	1.419	1.417	1.416	1.420	1.416	1.423	1.417
O_2–C_3	1.437	1.409	1.413	1.406	1.408	1.409	1.411	1.410	1.423	1.417
C_3–C_4	1.515	1.519	1.529	1.515	1.521	1.521	1.518	1.515	1.528	1.514
C_4–O_5	1.432	1.441	1.439	1.436	1.425	1.422	1.436	1.422	1.419	1.421
O_5–C_6	1.434	1.446	1.430	1.430	1.411	1.407	1.429	1.413	1.418	1.412
C_6–C_7	1.516	1.514	1.516	1.515	1.527	1.516	1.512	1.519	1.521	1.518
C_7–O_8	1.434	1.433	1.435	1.435	1.438	1.435	1.429	1.436	1.429	1.436
O_8–C_9	1.432	1.432	1.436	1.435	1.430	1.429	1.431	1.442	1.413	1.429
C_9–C_{10}	1.515	1.516	1.516	1.514	1.516	1.514	1.520	1.515	1.521	1.512
C_{10}–O_{11}	1.437	1.433	1.429	1.429	1.436	1.435	1.420	1.428	1.442	1.429
O_{11}–C_{12}	1.434	1.430	1.432	1.430	1.436	1.435	1.426	1.423	1.446	1.431
C_{12}–C_{13}		1.515	1.520	1.519	1.516	1.514	1.511	1.516	1.516	1.519
C_{13}–O_{14}		1.437	1.427	1.429	1.429	1.429	1.419	1.427	1.427	1.420
O_{14}–C_{15}		1.433	1.431	1.426	1.432	1.430	1.420	1.425	1.435	1.426
C_{15}–C_{16}			1.518	1.517	1.520	1.519	1.515	1.514	1.517	1.510
C_{16}–O_{17}			1.432	1.428	1.427	1.430	1.436	1.425	1.433	1.418
O_{17}–C_{18}			1.430	1.430	1.430	1.426	1.425	1.426	1.430	1.423
C_{18}–C_{19}					1.518	1.517	1.515	1.516	1.514	1.513
C_{19}–O_{20}					1.432	1.429	1.426	1.424	1.447	1.441
O_{20}–C_{21}					1.430	1.430	1.428	1.425	1.441	1.423
C_{21}–C_{22}								1.513	1.519	1.515
C_{22}–O_{23}								1.433	1.410	1.427
O_{23}–C_{24}								1.431	1.422	1.428
O_2–Li	1.992									
O_5–Li	2.015	1.979	2.086	2.037			2.087			
O_8–Li		2.019	2.062	2.070	2.065	2.043	2.221	2.066		2.084
O_{11}–Li	2.015	2.026	2.159	2.169	2.057	2.076	2.533	2.431	2.027	2.218
O_{14}–Li	1.992	2.026	2.013	2.019	2.144	2.186	2.604	2.211	1.986	2.529
O_{17}–Li			2.240	2.311	2.003	2.020	2.085	2.221	2.027	2.672
O_{20}–Li					2.230	2.285	2.192	2.486	2.013	2.077
O_{23}–Li								2.095		2.165

Table 6 Binding energies (ΔE) in kJ mol^{-1} of the conformers of $CH_3O(CH_2CH_2O)_nCH_3$– Li^+ (n = 3–7)

	Δ E
T_2	461.2
Te_2	461.7
P_2	481.7
P_3	490.8
H_2	481.9
H_3	490.5
H_4	495.0
Hp_1	500.3
Hp_3	472.9
Hp_4	528.6

1,200–1,150 cm^{-1} region. In brief the vibrational spectra provide insights for the cation polymer interactions in solid polymer electrolytes.

Experimental infrared and Raman spectra of $(PEO)_6$–Li^+ X^- (X= PF_6, AsF_6, SbF_6 and ClO_4), with the lithium ion showing hexadentate coordination, are reported in the literature [37]. As may be noticed readily the B3LYP vibrational frequencies of the $CH_3O(CH_2CH_2O)_nCH_3$–Li^+ (with n = 3–7) agree well with those in observed spectra reported in Ref. [37]. For example, a near doublet at the 1,394 and 1,387 cm^{-1} in the measured infrared spectra of $P(EO)_3LiX$ system can be correlated with the 1,397 and 1,380 cm^{-1} vibrations in the present calculations. These, however, are assigned to the CH_2 rocking vibrations. The 1,282 and 1,231 cm^{-1} CH_2 twist bands in the measured spectra are also in good agreement with the vibrations at 1,275 and 1,223 cm^{-1}, respectively, from the B3LYP theory. A near triplet (1,136, 1,110, 1,090 cm^{-1}) of C–O stretching vibrations observed in experiment agrees well with the calculated infrared spectra and these bands correspond to the 1,139, 1,110 and 1,096 cm^{-1} vibrations as reported in Table 8. It should be pointed out here that the experimental infrared

Table 7 Selected B3LYP vibrational frequencies for the lowest energy conformer of $CH_3O(CH_2CH_2O)_nCH_3$–Li^+ (n = 3–5)

Assignment	T_2	Li–T_2	Te_2	Li–Te_2	P_3	Li–P_3
CH_2 scissor	1,511 (20)	1,512 (21)	1,507 (24)	1,512 (20)	1,506 (41)	1,513 (14)
	1,507 (27)	1,497 (19)	1,505 (22)	1,488 (16)		
CH_2 rock	1,400 (71)	1,397 (39)	1,405 (24)	1,393 (49)	1,400 (57)	1,396 (54)
	1,385 (109)	1,380 (32)	1,394 (103)	1,378 (37)	1,391 (184)	1,385 (48)
			1,382 (70)		1,380 (46)	
CH_2 twist	1,232 (58)	1,275 (34)	1,280 (23)	1,335 (19)	1,276 (34)	1,276 (16)
		1,223 (17)	1,232 (28)	1,275 (30)	1,233 (23)	1,270 (20)
			1,219 (54)	1,232 (30)	1,197 (33)	1,228 (48)
CH_2 wag	1,192 (27)					
C–O stretch	1,182 (61)	1,155 (26)	1,188 (36)	1,169 (80)	1,187 (72)	1,175 (94)
	1,172 (206)		1,184 (23)		1,182 (91)	1,168 (24)
	1,161 (104)		1,183 (109)			1,157 (58)
	1,157 (254)					1,151 (102)
CH_2 wag		1,142 (33)	1,176 (60)	1,165 (40)	1,177 (51)	1,146 (46)
			1,173 (180)		1,173 (242)	
					1163 (324)	
C–O stretch		1,139 (190)	1,163 (121)	1,155 (40)	1,158 (68)	1,136 (361)
			1,155 (179)		1,150 (76)	
					1,143 (38)	
CH_2 wag		1,121 (87)	1,145 (27)	1,141 (30)		1,124 (30)
			1,130 (20)			
C–O stretch		1,110 (376)		1,138 (170)		1,112 (144)
		1,096 (34)				
CH_2 wag				1,121 (68)		1,098 (130)
C–O stretch				1,109 (398)		
				1,096 (52)		
				1,088 (47)		
CC + CO stretch	1,052 (30)	1,087 (36)	1,088 (27)	1,062 (24)	1,085 (28)	1,055 (36)
		1,038 (25)	1,057 (31)	1,050 (39)	1,057 (37)	1,048 (24)
		1,028 (27)	992 (37)	1,029 (24)		1,035 (28)
CH_2 wag	971 (37)	958 (49)	970 (37)	958 (53)	969 (42)	967 (31)
		856 (34)	965 (34)	934 (20)	880 (31)	960 (39)
			880 (22)	865 (26)	869 (26)	954 (30)
			874 (27)		862 (26)	865 (36)
Li–O stretch		522 (120)		523 (34)		473 (92)
				508 (98)		

and Raman spectra of $(PEO)_6$–LiX has also been reported in Ref. [37]. Here again a near doublet at 1,131 and 1,111 cm^{-1} has been predicted from the B3LYP calculations. A 13 cm^{-1} separation for the corresponding bands (1,127 and 1,114 cm^{-1}) has been observed in the infrared spectra (Ref. [37]). Similarly the 1,089, 1,075 and 954 cm^{-1} vibrations in an experiment are well correlated to (1,097, 1,065 and 951 cm^{-1}) frequencies of normal vibrations obtained from the B3LYP theory.

In brief, the characteristic normal vibrations in $CH_3O(CH_2$-$CH_2O)_nCH_3$–Li^+ (n = 3–7) modeled systems provide insights for the ion pair formation or cation–polymer interactions in the solid polymer electrolytes.

4 Conclusions

Systematic investigations of electronic structure, molecular electrostatic potentials and the vibrational frequencies in $CH_3O(CH_2CH_2O)_nCH_3$–Li^+ (n = 3–7) have been presented. The conclusions of this work are summarized below. (1) Lowest energy conformers of $CH_3O(CH_2CH_2O)_nCH_3$ (n = 3–6) prefer to have *trans*-conformation around the C–C bonds. For heptaglyme, however, the energetically favourable structure turns out to be the one having *gauche*-conformation around the C–C bonds. (2) MESP topography provides a systematic approach to derive different structures of $CH_3O(CH_2CH_2O)_nCH3$–Li^+ (n = 3–7) ion pairs. (3) For the $CH_3O(CH_2CH_2O)_nCH_3$–Li (n = 3–7) ion pairs the lowest energy structure presents a *gauche*-conformation around the C–C bonds of the polyether framework, which can be explained from the MESP topography. The volume enclosed by an MESP isosurface in different $CH_3O(CH_2CH_2O)_nCH_3$ (n = 3–7) conformers is relatively large when the *gauche*-conformation around the C–C bonds is obtained. (4) Heptaglyme exhibiting deepest MESP minimum near ether oxygen predicts largest cation binding energy. (5) The CH_2 bending and the C–O stretching vibrations of the PEO oligomers (n = 3 and n = 6 in the above series) agree well with the experimental spectra. Analysis of normal vibrations in the

Table 8 Selected B3LYP vibrational frequencies for the lowest energy conformer of $CH_3O(CH_2CH_2O)_nCH_3–Li^+$ ($n = 6–7$)

Assignment	H_4	Li–H_4	Hp_4	Li–Hp_4
CH_2 scissor	1,507 (23)	1,511 (22)	1,507 (23)	1,511 (16)
	1,505 (28)		1,505 (28)	1,506 (17)
CH_2 rock	1,401 (30)	1,406 (24)	1,401 (30)	1,405 (42)
	1,393 (168)	1,398 (90)	1,393 (168)	1,393 (114)
	1,387 (143)	1,392 (35)	1,387 (143)	1,388 (36)
	1,379 (24)		1,379 (24)	
CH_2 twist	1,280 (33)	1,337 (19)	1,280 (33)	1,336 (20)
	1,275 (21)	1,283 (27)	1,276 (21)	1,284 (30)
	1,232 (24)	1,277 (21)	1,232 (24)	1,280 (36)
	1,232 (25)	1,234 (26)	1,231 (25)	1,228 (31)
C–O stretch	1,188 (41)	1,182 (37)	1,200 (35)	1,183 (80)
	1,185 (45)	1,169 (110)	1,188 (41)	1,182 (33)
	1,181 (51)		1,185 (185)	
			1,181 (51)	
CH_2 wag	1,179 (52)	1,166 (27)	1,179 (52)	1,167 (40)
	1,175 (146)		1,175 (146)	
	1,168 (163)			
C–O stretch	1,150 (60)	1,159 (110)	1,168 (163)	1,160 (43)
		1,150 (176)		1,159 (143)
				1,150 (103)
				1,147 (132)
CH_2 wag	1,144 (51)	1,131 (88)	1,164 (287)	1,141 (69)
	1,141 (24)			1,140 (126)
	1,114 (21)			
C–O stretch		1,119 (22)	1,159 (117)	1,131 (193)
		1,111 (157)	1,152 (118)	1,121 (26)
				1,108 (136)
				1,105 (163)
				1,096 (45)
CH_2 wag		1,106 (99)	1,150 (60)	
		1,097 (72)	1,144 (51)	
			1,114 (21)	
CC + CO stretch	1,087 (17)	1,082 (45)	1,056 (38)	1,081 (41)
		1,065 (25)		1,049 (27)
		1,041 (50)		
CH_2 wag	977 (58)	970 (41)	977 (58)	970 (51)
	975 (52)	951 (36)	975 (52)	968 (20)
	877 (24)	871 (47)	877 (27)	966 (22)
	866 (36)	862 (23)	866 (36)	944 (27)
	861 (26)		861 (26)	874 (59)
				857 (22)
Li–O stretch		424 (21)		422 (35)
		384 (49)		

present series demonstrates that the C–O stretching vibrations comprised of oxygen atoms interacting with the lithium ion can be correlated qualitatively with the strength of O–Li interactions.

Acknowledgements SPG thanks the Council of Scientific and Industrial Research [Project 01(1772) / 02 / EMR-II], New Delhi, India for the financial support.

References

1. Gejji SP, Hermansson K, Tegenfeldt J, Lindgren J (1993) J Phys Chem 97:11402
2. Gejji SP, Suresh CH, Babu K, Gadre SR (1999) J Phys Chem 103:7474
3. Rey L, Johansson P, Lindgren J, Lassegues JC, Grondin J, Servant L (1998) J Phys Chem A 102:3249
4. Lauenstein A, Tegenfeldt J (1998) J Phys Chem B 102:6702

5. Bruce PG, Gray FM (1995) Solid state electrochemistry. Cambridge University Press, New York, p 119
6. MaeCallum JR, Vincent CA (1987) Polymer electrolyte reviews-I. Elsevier, London
7. Redfern PC, Curtiss LA (2002) J Power Sources 110:401
8. Sutjianto A, Curtiss LA, (1998) J Phys Chem A 102:968
9. Frech R, Huang W (1994) Solid State Ionics 72:103
10. Addison CC, Amos DW, Sutton D (1968) J Chem Soc 2285
11. Burger K (1983) Studies in analytical chemistry 6: salvation and complex formation reactions in non-aqueous solvents. Elsevier, Amsterdam
12. Papke BL, Ratner MA, Shiver DF (1982) J Electrochem Soc 129:1694
13. Ratner MA, Shriver DF (1988) Chem Rev 88:1988
14. Gejji SP, Johansson P, Tegenfeldt J, Lindgren J (1995) Comput Polym Sci 5:99
15. Bruce PG, Vincent CA (1993) J Chem Soc Faraday Trans 89:3187
16. Bhattacharja S, Smoot SW, Whitmore DH (1986) Solid State Ionics 18&19:306
17. Arumugam S, Shi J, Tunstall DP, Vincent CA (1993) J Phys Condens Matter 5:153
18. Boden N, Leng SA, Ward IM (1991) Solid State Ionics 45:261
19. Johansson P, Gejji SP, Tegenfeldt J, Lindgren J (1996) Solid State Ionics 86–88:297
20. Johansson P, Tegenfeldt J, Lindgren J (1999) Polymer 40:4399
21. Frech R, Huang W (1995) Macromolecules 28:1246
22. Gejji SP, Gadre SR, Barge VJ (2001) Chem Phys Lett 344:527
23. Matsuura H, Fukuhara K, Tamaoki H (1987) J Mol Struct 156:293
24. Matsuura H, Fukuhara K (1986) J Polym Sci B 24:1383
25. Matsuura H, Miyazawa T, Machida K (1973) Spectrochimca Acta 29A:771
26. Frech R, Huang W (1994) Solid State Ionics 72:103
27. Johansson P, Tegenfeldt J, Lindgren J (1998) J Phys Chem A 102:4660
28. Arnaud R, Benrabah D, Sanchez JY (1996) J Phys Chem 100:10882
29. Gadre SR, Bhadane PK, Pundlik SS, Pingale SS (1996) In: Murray JA, Sen K (eds) Molecular electrostatic potentials: concepts and applications. Elsevier, Amsterdam, p 219
30. Suresh CH, Gadre SR, Gejji SP (1998) Theor Chem Acc 99:151
31. Gejji SP, Suresh CH, Bartolotti LJ, Gadre SR (1997) J Phys Chem A 101:5678
32. Gejji SP, Agrawal PR, Dhumal NR (2002) Theor Chem Acc 107:351
33. GAUSSIAN03 package: Frisch MJ, Trucks GW, Schlegel HB, Scuseria GE, Robb MA, Cheeseman JR, Montgomery JA, Vreven T Jr, Kudin KN, Burant JC, Millam JM, Iyengar SS, Tomasi J, Barone V, Mennucci B, Cossi M, Scalmani G, Rega N, Petersson GA, Nakatsuji H, Hada M, Ehara M, Toyota K, Fukuda R, Hasegawa J, Ishida M, Nakajima T, Honda Y, Kitao O, Nakai H, Klene M, Li X, Knox JE, Hratchian HP, Cross JB, Adamo C, Jaramillo J, Gomperts R, Stratmann RE, Yazyev O, Austin AJ, Cammi R, Pomelli C, Ochterski JW, Ayala PY, Morokuma K, Voth GA, Salvador P, Dannenberg JJ, Zakrzewski VG, Dapprich S, Daniels AD, Strain MC, Farkas O, Malick DK, Rabuck AD, Raghavachari K, Foresman JB, Ortiz JV, Cui Q, Baboul AG, Clifford S, Cioslowski J, Stefanov BB, Liu G, Liashenko A, Piskorz P, Komaromi I, Martin RL, Fox DJ, Keith T, Al-Laham MA, Peng CY, Nanayakkara A, Challacombe M, Gill PMW, Johnson B, Chen W, Wong MW, Gonzalez C, Pople JA (2004) Gaussian, Inc., Wallingford CT
34. Limaye AC, Gadre SR (2001) Curr Sci (India) 80:1298
35. Becke D (1993) J Chem Phys 98:5684
36. Lee C, Yang W, Parr RG (1988) Phys Rev B37:785
37. Ducasse L, Dussauze M, Grondin J, Lassegues JC, Naudin C, Servant L (2003) Phys Chem Chem Phys 5:567